PROGRESS IN COLOR, COLORANTS AND COATINGS

available online @ www.pccc.icrc.ac.ir

Ministry of Science, Research and Technology
Institute for Color Science & Technology

Progress in Color Colorants Coating 16 (2023), 181-195

High Durable Latex-Modified-Concretes: The Effect of Minimum Film Formation Temperature of Acrylic-Styrene Latex

S. Abdollahi Baghban, M. Khorasani*
Department of Polymer and Color Engineering, Amirkabir University of Technology, P.O. Box: 15875-4413, Tehran, Iran.

ARTICLE INFO

Article history:
Received: 25 June 2022
Final Revised: 05 Nov 2022
Accepted: 06 Nov 2022
Available online: 07 Feb 2023

Keywords:
Minimum film formation temperature
Durability
Acrylic-styrene latex
Non-steady-state migration coefficient
Rapid chloride migration test
Concrete.

ABSTRACT

This paper aimed to investigate the effect of the minimum film formation temperature (MFFT) of acrylic-styrene latexes (ASL) on the durability, physical, and mechanical characteristics of latex-modified concretes (LMCs). LMCs were designed and manufactured incorporating three ASLs with different MFFTs, namely 0, 8, and 25 °C (Water/Cement mass ratio=0.445 and latex/water mass ratio=0.05). Water absorption (WA), rapid chloride ion migration, carbonation, compressive-splitting tensile strength, and scanning electron microscopy (SEM) were employed to study LMCs properties. The performance of LMCs was found to be dependent on the MFFT of the latexes strongly. The results revealed that LMCs containing ASL with lower MFFT compared to ambient temperature (MFFT<25 °C) had a lower slump, compressive and tensile strength, and higher WA, chloride ion, and CO_2 penetration due to the higher film formation rate of latexes on the non-hydrated cement particles and the decreased final hydration degree. Furthermore, it was indicated that chloride penetration, water adsorption, and tensile strength of LMCs containing latexes with high MFFT (MFFT>25 °C) decreased by 14 %, 10 and 20 % compared to the conventional concrete, respectively. Such a chloride penetration reduction is a great achievement. Accordingly, carboxylated alkaline ASLs with high MFFT can be a promising candidate for preparing the LMCs, which can be applied in reinforced concrete in corrosive conditions. Prog. Color Colorants Coat. 16 (2023), 181-195© Institute for Color Science and Technology.

1. Introduction

In recent decades, concrete has attracted much attention due to being compressive, fire-resistant, moldable, inexpensive, accessible, etc. [1, 2]. Concrete possesses outstanding characteristics even though its applications have been limited due to its relatively high permeability to aggressive agents such as chloride ions and low tensile strength (TS) [3, 4]. Reinforced concrete (RC) has been employed as an effective proposed solution to improve the TS of concrete structures. Moreover, the tendency of RC to crude due to the chloride attack, especially in the marine environment, and carbonate attack in urban zones is a controversial topic [5, 6]. RC corrosion usually has two stages, the initiation phase related to the ions penetration up to the reinforcement and propagation phase associated with the corrosion of embedded

*Corresponding author: * khorasani.m@aut.ac.ir
Doi: 10.30509/pccc.2022.166996.1174

steels, concrete cracking, and spalling [7, 8]. The corrosion resistance of concrete strongly depends on the hydration reaction between water and cement particles, producing $Ca(OH)_2$. The excessive amount of $Ca(OH)_2$ prevents the corrosion of RCs by providing a passive environment; however, this safe condition can be destroyed due to the ion attacks [9, 10].

Different types of polymer materials, such as water-based latexes, have been considered to improve their performance and especially control their corrosion rate [11-16]. Latex-modified concretes (LMCs) can be manufactured by replacing a part of other conventional ingredients with latex [17, 18]. Latex resins are colloidal dispersions of polymer particles in water, generally produced by emulsion polymerization [19-23]. Pei et al. claimed that covering the aggregates with the latex-modified cement paste in concrete provides superior properties to conventional concrete [12]. Gao et al. examined the effect of combining the polyacrylic ester (PAE) and silica fume (SF) with cement mortar on the mechanical and durability properties. It was observed that PAE-SF-modified mortars had superior characteristics to ordinary cement mortars [24]. Joo et al. achieved modified concrete with excellent mechanical properties using styrene-butadiene rubber (SBR) [25]. Kwon et al. reported that modified mortars with high strength could be obtained by combining the slag and acrylic emulsions [20].

Furthermore, Almeida investigated the effect of applying styrene-acrylate latex in the SF-modified mortars and found that their bond and mechanical strength were enhanced compared to ordinary mortars [19]. Hence, nowadays, elastomeric latexes based on acrylic-styrene-butadiene and acrylic-styrene copolymers are commonly employed in commercial LMCs to endow desirable properties. Although there are many reports on the suitable performance of these LMCs containing latexes such as polyvinyl acetate or polyvinylidene chloride, some studies expressed that using latexes in concrete mixtures reduces their corrosion and wet mechanical strength [26, 27]. Thus, it cannot be concluded that all acrylic-styrene-latexes (ASLs) have appropriate effects on LMCs. Despite the researchers' efforts, there have been limited reports on the finding the influence of resin structure and properties on LMCs, and driving parameters to determine the most appropriate latex was not found. Notably, the hydration reaction and latex film formation in these systems is very complex, and comprehensive studies are required to understand the leading factors well. Herein, the effect of minimum film formation temperature (MFFT) and glass transition temperature (Tg) of ASLs on the penetration, durability, physical, and mechanical characteristics of the prepared LMCs are investigated by different methods to identify the governing parameters to find the best latex.

2. Experimental

2.1. Materials

Ordinary Portland cement (OPC) (Type III) was prepared from Abyek Cement Co. (Iran), and its properties are listed in Tables 1 and 2. Natural crushed and washed river sand with a fineness modulus of 3.85 (size: 9.5 mm or finer), and fineness modulus of 6.14 (size: 12.5 mm or finer) ASTM C 33 were employed from Abrar shen (Iran) as fine and coarse aggregates, respectively with a mass ratio of coarse to fine of 30:70. Specific gravity (AASHTO T 84), evaporable moisture content (ASTM C 566), and water absorption (WA) (ASTM C 128) of aggregates were measured and mentioned in Table 3. ASLs with different MFFT (0, 8, and 30 ºC) and Tg values (-2, 16, and 25 °C) were purchased from Simab Resin Co. (Iran) and used to produce LMC samples. The chemical and physical characteristics of these latexes are revealed in Table 4. Silicone-emulsion-type anti-foamer, $Ca(OH)_2$, and silver nitrate ($AgNO_3$) were supplied from Merck Co.

Table 1: Physical properties of OPC.

Compressive strength (MPa)			Setting time (min)		Density (kg/m^3)	Specific surface (Blaine) (Cm^2/gr)	Fineness#200
1 day	7 days	28 days	final	Initial			
17	34	40.3	235	180	3150	3300	1.28 %

Table 2: Chemical composition of cement.

Component	Mass percent (%)
Lime (CaO (C))	64.80
Silica (SiO_2 (S))	21.2
Alumina (Al_2O_3 (A))	5.32
Ferric oxide (Fe_2O_3 (F))	2.7
Magnesia (MgO (M))	2.6
Alkalis (K_2O (K))	0.61
Alkalis (Na_2O (N))	0.34
Sulfur trioxide (SO_3 (S))	2.42
Carbon dioxide (CO_2 (C))	0
Water (H_2O (H))	0
C_3S	56.43
C_2S	15.28
C_3A	10.53
C_4AF	8.33

Table 3: Size, specific gravity, water absorption, and evaporable moisture content of fine and coarse aggregates.

Aggregates	Maximum size (mm)	Fineness modulus	Specific gravity (kg/m^3)	Water absorption (%)	Evaporable moisture content (%)
Fine aggregate	9.5	3.85	2.56	1.84	3.04
Coarse aggregate	12.5	6.14	2.58	2.24	0.54

Table 4: Characteristics of water-based acrylic-styrene copolymer latexes.

Properties	ASL-1	ASL-2	ASL-3
pH	6-8	8-10	9-10
MFFT (°C)	0	8	25
Tg (°C)	-2	16	25
Solid content (%)	50 ±1	50 ±1	50±1
Density (g/cm^3)	1.075	1.030	1.05
Viscosity by Brook Field (cP)	9500	9200	9450
Chemical composition	Styrene-Acrylic	Styrene-Acrylic	Styrene-Acrylic
Emulsifying system	Anionic	Anionic	Anionic

2.2. Mixture proportion design and specimen preparation

The composition of the four mix designs of LMCs, including MC1, MC2, MC3, and MC4, is demonstrated in Table 5. LMC samples were produced with a water-to-cement (W/C) mass ratio of 0.445 and a solid latex content-to-cement (L/C) mass ratio of 0.05. First, an anti-foamer was added to the latex to prevent making foams in LMCs. No more additives were used due to their influence on the general properties of LMCs. Then, the ingredients were mixed in a concrete mixer for 15 minutes. According to the procedures outlined in ASTM C 39, cubic and cylinder specimens were cast and demolded after 24 hours. All specimens were cured in humid conditions for 28 days.

2.3. Testing method

Cement, latex, and water were mixed in the proportion described in Table 5, and the pH values of mixtures were identified by laboratory pH meter (Knick 765) as soon as possible. The slump was measured based on ASTM C 143 to signify the workability and fluency of fresh concrete. Also, the density of concrete samples was identified according to ASTM C 1688M 14. Moreover, initial and final setting times were measured according to ASTM C 191 to detect how latexes affect the hydration reaction rate. Compressive strength and splitting tensile tests were carried out based on ASTM C 39 and ASTM C 78, respectively. All of the measurements were repeated triplicates, and average values were reported.

Cylindrical LMC specimens from each mixture (ϕ 100 × 200 mm) were moist-cured for 28 days and employed for rapid chloride migration test (RCMT) according to Nord Test (NT) build 492 standard (1999-11). Test specimens were prepared by cutting the cylinders into 50±2 mm thick slices with the diamond blade. Before migration tests, all the specimens were vacuum-saturated with saturated calcium hydroxide $Ca(OH)_2$ solution. RCMT was conducted based on the forced ionic migration induced by the external electrical voltage applied across the $Ca(OH)_2$ saturated LMC samples. Due to the potential differences between the anode and cathode electrodes, chloride ions migrated from the upstream solution (NaCl, 10 wt. %), through the LMC samples, towards the downstream solution (NaOH, 0.3 N) for a determined time (see Figure S1 in the supplementary information (SI)). Next, samples were split into two parts. Then, the penetration depth of chloride ions was recognized by spraying $AgNO_3$ solution (0.1 N) and measured by calipers at 7 points. The average penetration depths calculated non-steady-state chloride ion migration coefficients according to Equation 1.

$$D_{nssm}=\frac{0.0239(273+T)L}{(u-2)t}\times(x_d-0.0238\sqrt{\frac{(273+T)\times L\times X_d}{u-2}}) \qquad (1)$$

Table 5: Mix proportion design of LMC samples.

Mix design	MC1	MC2	MC3	MC4
Acrylic-styrene-latex	-	ASL-3	ASL-2	ASL-1
Water to cement mass ratio (W/C)	0.445	0.445	0.445	0.445
latex solid content to cement mass ratio (L/C)	0.05	0.05	0.05	0.05
Cement Content ($\frac{kg}{m^3}$)	431.47	431.47	431.47	431.47
Fine aggregates ($\frac{kg}{m^3}$)	1224.31	1224.31	1224.31	1224.31
Coarse aggregate ($\frac{kg}{m^3}$)	400.99	400.99	400.99	400.99
Water content ($\frac{kg}{m^3}$)	196.87	175.29	175.29	175.29
Latex ($\frac{kg}{m^3}$)	0	43.147	43.147	43.147

Where, D_{nssm} is a non-steady-state migration coefficient *[m^2/s]*; *u* is the absolute value of the applied voltage *[V]*; *T* is the average value of the initial and final temperatures in the anolyte solutions *[K]*; *L* is the thickness of the specimen *[m]*; x_d is the average value of the penetration depths *[mm]*, and *t* is test duration *[s]* [28, 29]. Measurements were repeated in triplicates to acquire an average value.

Carbonation depth was measured according to the RILEM CPC 18 procedure. Cubic LMC samples (10×10×10 cm^3) were cast and demolded after 24 hours, polished, and cleaned to conduct the carbonation tests. Next, samples were stored for six days in a fog room (21 °C and 98 % RH), three hours at 50±5 °C and 50±10 % RH to stabilize and reduce internal humidity, followed by seven days in a chamber with 23±2 °C and 65±5 % RH. Finally, carbonation tests were accomplished in the carbonation chamber (23±2 °C, RH of 65±5 %, and CO_2 gas effective concentration of 10 %). Carbonation depth was determined after 7, 14, and 28 days of exposure to the carbonation condition using phenolphthalein (pH indicator 8.2-9.8) and thymolphthalein (pH indicator 9.3-10.5). The carbonation constants of samples were estimated according to Equation 2 using the carbonation depth as a function of time.

$$e_{CO_2} = k_{CO_2} \times \sqrt{t} \quad (2)$$

Where, e_{co2} is the carbonation depth *[mm]*, k_{co2} is carbonation constant *[mm/year$^{1/2}$]*, and *t* is exposure time *[year]*. The averaged values were reported after three measurements.

The capillary water adsorption (I) was found according to ASTM C 1585 04 based on the mass increment. Before dipping the samples in the water, the around surfaces of cylindrical specimens were sealed by epoxy resin. WA was calculated by Equation 3.

$$I = \frac{m_I}{a \times b} \quad (3)$$

Where *I* is the CWA *[mm]*, m_I is the mass change at time *t [g]*, *a* is the exposed cross-sectional area of the specimen to the water *[mm^2]*, and *b* is the density of the water *[g/mm^3]*. Besides, cubic specimens (10×10×10 cm^3) were dried at 105 °C for 72 hours, cooled for 24 hours, weighted, and immediately immersed in the water container for certain times, and finally reweighted to obtain WA (British Standard 1881 122). Measurements were repeated in triplicates to acquire an average value.

The cross-sectional and silicon X-ray mapping micrographs were attained to signify the morphology of LMC samples and the location of latex films throughout the samples by using scanning electron microscopy coupled with an energy dispersive X-ray spectrometer (SEM-EDX) (QUANTA INSPECT F SEM device equipped with a field emission gun, 1.2 nm resolution, 5.0 kV). To this, aged LMC specimens were crushed into small pieces and coated with gold to observe the latex film formation (LFF).

3. Results and Discussion

The appearance of the MC4 containing ASL-1 after 28 days was illustrated in Figure 1. As can be seen in Figure 1, MC4 didn't have any coherent structure and could not be moldable after 28 days. It was observed that the cement-latex paste of MC4 containing ASL-1 didn't have any adhesion tendency to the aggregates during the mixing; even this behavior could not be remedied by adding more water or continuing the mixing (Figure S2 in the SI). Consequently, MC4 was omitted from the rest of the experimental tests.

As reported in Table 6, the pH values of all LMCs were higher than 11.5. According to previous studies, a passive layer can be formed on the steel rebar in an alkaline environment (pH>11), which protects it from corrosion caused by the penetration of oxygen, water,

Figure 1: MC4 after 28 days of moisture-curing in humid conditions.

and aggressive agents such as chloride ions. If the pH value of concrete is less than 11.5, the passive layer on the embedded steel will be destroyed, and corrosion may occur rapidly without the presence of chloride. In contrast, a significant amount of chloride is required to initiate the corrosion at pH values greater than 11.5 [30-32]. Accordingly, the latex-modified mortar media is not corrosive for embedded steels in LMCs.

All of the mix designs were adjusted for the slump of 80±10 mm; however, the use of latexes in concrete formulation changed their slump values compared to MC1. The results demonstrated that different ASLs acted differently; ASL-2 and ASL-3 increased the fluency of fresh LMCs significantly and acted as a superplasticizer, even at low water-to-cement mass ratios of 0.445, while ASL-1 decreased the slump of MC4.

According to Table 5, the density of LMCs was reduced by using the latexes. It can be associated with the lower density of latexes compared to the other ingredients and the existence of some voids and gaps. MC4 containing ASL-1 had the lowest density due to the high number of voids. They can reduce the cohesivity and mechanical strength of MC4, as can be seen in Figure 1. The cross-sectional view of MC1 (without latex), MC2 containing ASL-3, and MC3 containing ASL-3 are illustrated in Figure 2. As can be seen in Figure 2 (C), MC3 has a high amount of entrapped air and voids. It is noteworthy that a balance between density reduction and maintaining the structural cohesion of the concrete must be provided so that the concrete structure is not become too porous by the density reduction. Hence, the density reduction of MC2 (-10 %) was more reasonable rather than MC4 (-12 %) and MC3 (-17 %). So, MC2 is an appropriate candidate for manufacturing light constructions.

According to Table 5, the use of ASL-2 and ASL-3 increased the initial and final setting time of latex-modified mortars compared to the control sample (MC1), while ASL-1 decreased these time values. The compressive strength of LMCs after 7, 28, 56, and 90 days of casting are depicted in Figure 3 and Table 6.

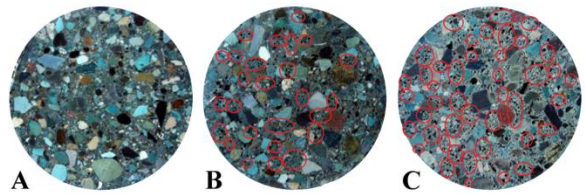

Figure 2: The cross-sectional view of concrete samples: A) MC1, B) MC2, and C) MC3.

Table 6: Physical and mechanical properties of LMC samples.

Characteristics	MC1	MC2	MC3	MC4
pH	12.82	12.26	11.89	11.62
Slump (mm)	85	185	170	70
Density (g/m^3)	2.307	2.086	2.031	1.920
Decreased density compared to fresh concrete (%)	0	-10	-12	-17
Initial setting time	180	250	190	110
Final setting time	235	270	245	175
Compressive strength at 7 days (MPa)	25.7±2	18.7±2	11.6±2	-
Compressive strength after at 28 days (MPa)	38.6±2	29.6±2	13.5±2	-
Compressive strength after at 56 days (MPa)	41±2	31.1±2	14.6±2	-
Compressive strength after at 90 days (MPa)	41.5±2	34±2	16±2	-
Splitting tensile strength (MPa)	2.44±0.2	2.5±0.2	1.97±0.2	-

According to the results figured out in Figure 3, it is obvious that the compressive strengths of the LMCs decrease with latex addition due to the disorders in a hydration reaction. As can be seen in Table 6, the compressive strength increased in the order of MC1> MC2>MC3. Furthermore, Figure 3 exhibits that the compressive strength growth of MC2 is similar to MC1. These results were not following the published reports by Bahranifard et al., which indicated that the mechanical properties of the concrete were improved significantly by adding styrene-butyl acrylate latex [26]. Conversely, the obtained results agreed with those Divry et al. reported [27].

Results in Table 6 signified that the increment trend of splitting tensile strength values is MC2>MC1>MC3; in other words, MC2 has higher splitting tensile strength. Therefore, using ASL-3 in concrete enhanced the splitting tensile strength. Figure 4 illustrates the cross-section image of concrete specimens exposed to the chloride solution in which their chloride ion penetration depth can be identified. According to Table 6, the average of non-steady-state migration coefficients of chloride ions (D_{nssm}) of MC1, MC2, and MC3 are 2.023886×10^{-11}, 1.739082×10^{-11}, and 2.311171×10^{-11} [m^2/s], respectively. Therefore, MC2 has the minimum D_{nssm} showing that MC2 is more impermeable to chloride migration. Consequently, MC2 delays the corrosion of embedded steel well compared to MC1 and MC3. Generally, the penetration probability of chloride ions is related to the electrochemical condition inside the concrete directly [33]. Both the diffusion coefficient through the pore solution and the physical characteristics of the capillary pore structure control the diffusion rate of chloride ions [34]. The average carbonation depths of each specimen after 21, 28, and 42 days of exposure to the carbonation conditions were mentioned in Table 8 (Figures S3 and S4).

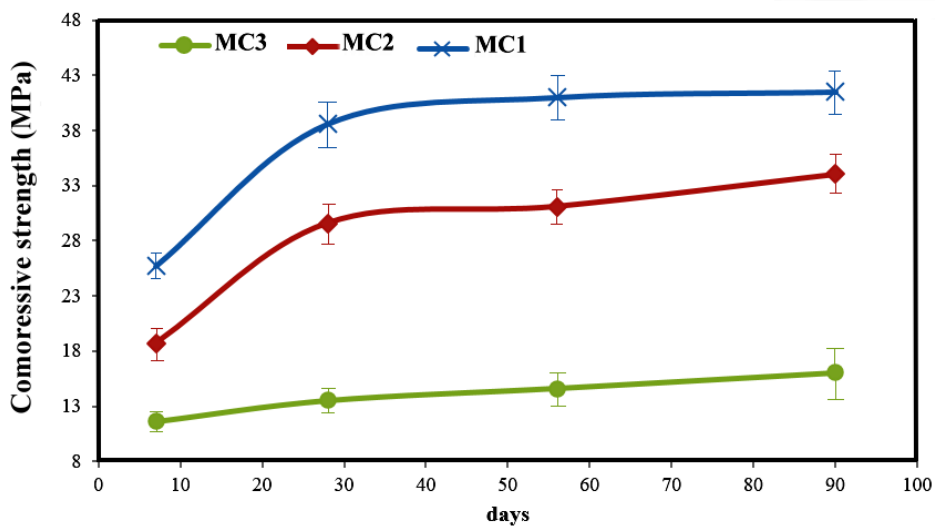

Figure 3. Compressive strength of MC1, MC2, and MC3.

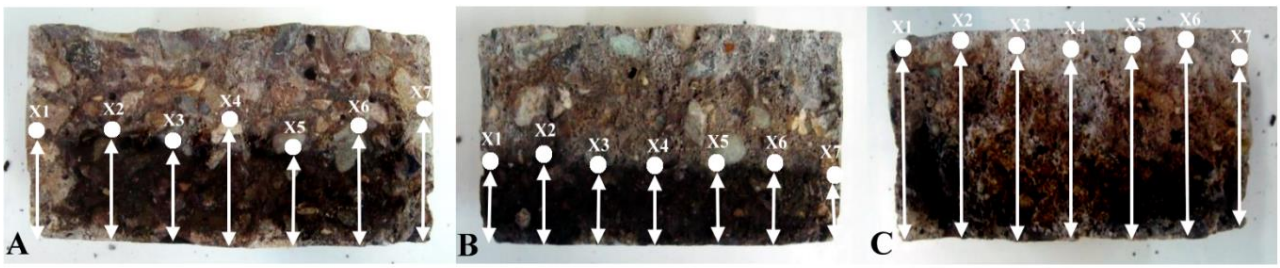

Figure 4: Chloride diffusion depth of: A) MC1, B) MC2, and C) MC3 in RCMT.

It was observed that carbonation did not occur in MC2 and MC3 even after 42 days of exposure to carbonation conditions. The carbonation depth of MC1 was clear, and this depth had been growing during the carbonation time.

Diffusion of chloride and carbonate ions into concretes depends on water in pores, so the penetration can only occur in the concrete pores containing partly water. In other words, CO_2 diffusion occurs very slowly if pores are full of water, while CO_2 remains in the gaseous state and does not have to destroy behavior if pores are rather dry. Accordingly, a little moisture penetration from an external source is essential to carbonate the concrete; i.e., CO_2 reacts with water in the presence of an adequate amount of moisture, and carbonic acid forms, which reduces the alkalinity of concrete and produces $CaCO_3$ as the result of the reaction of the carbonic acid and $Ca(OH)_2$. It is worth noticing that the pH value will reduce up to about 8 when all of the $Ca(OH)_2$ has become carbonated. In such a low pH value, the passive protective layer gets destroyed, and the steel begins to corrode. The highest carbonation rate happens at a relative humidity of 50-70 % [32, 34]. Also, the WA of concrete depends on many factors, including concrete mixture proportions, the presence of micro and macro cracks, the entrapped air content, the physical and chemical characteristics of the ingredients, the degree of hydration, the curing time, the surface treatments, and the moisture condition of the concrete at the time of testing [27-29, 32-35]. Hence, carbonation and chloride diffusion rate depend on concrete's WA as a governing parameter. The capillary water absorption (I) of samples is depicted in Table 9.

Table 7: The chloride diffusion depth, average migration coefficient of samples, and RCMT conditions.

Samples	Sample length (mm)	Time (hours)	Applied voltage (V)	Average of final and initial temperatures (°C)	Average chloride diffusion depth (mm)	Average migration coefficient $\times 10^{+11}$ (m^2/s)
MC1	49.67	24	25	24.39	31	2.04
MC2	48.92	24	25	24.13	28.4	1.74
MC3	46.67	24	25	25.38	42.12	2.31

Table 8: Carbonation depths were determined by phenolphthalein and thymolphthalein and the carbonation constant of specimens after 21, 28, and 42 days of exposure to the carbonation conditions.

Exposure time of carbonation condition	MC1	MC2	MC3
e_{CO_2} by phenolphthalein at 21 days (mm)	NCC*	NCC	NCC
K_{CO_2} by phenolphthalein at 21 days (mm/year$^{1/2}$)	–	–	–
e_{CO_2} by thymolphthalein at 21 days (mm)	NCC	NCC	NCC
K_{CO_2} by thymolphthalein at 21 days (mm/year$^{1/2}$)	–	–	–
e_{CO_2} by phenolphthalein at 28 days (mm)	4.6	NCC	NCC
K_{CO_2} by phenolphthalein at 28 days (mm/year$^{1/2}$)	1.27	–	–
e_{CO_2} by thymolphthalein at 28 days (mm)	5.3	NCC	NCC
K_{CO_2} by thymolphthalein at 28 days (mm/year$^{1/2}$)	1.47	–	–
e_{CO_2} by phenolphthalein at 42 days (mm)	7.5	NCC	NCC
K_{CO_2} by phenolphthalein at 42 days (mm/year$^{1/2}$)	2.54	–	–
e_{CO_2} by thymolphthalein at 42 days (mm)	8.7	NCC	NCC
K_{CO_2} by thymolphthalein at 42 days (mm/year$^{1/2}$)	2.96	–	–
NCC*: No color change			

Table 9: Capillary water absorption (I) of samples.

days	Time (s)	I of MC1	I of MC2	I of MC3
1	0	0	0	0
1	60	0.056	0.178	0.447
1	300	0.106	0.396	0.615
1	660	0.152	0.418	0.724
1	2220	0.222	0.612	0.931
1	3012	0.251	0.654	1.002
1	11520	0.418	0.924	1.509
2	162000	0.797	1.805	3.011
3	263556	1.029	2.329	3.9
4	349200	1.124	2.832	4.514
5	439200	1.211	2.92	4.887
6	529200	1.322	2.976	5.172
7	604800	1.355	3.0863	5.21

Table 10 and Figures S5-S7 in the SI shows that each sample has two WA regions with different slopes. The first region with a steep slope and the other with a gentle slope was recognized as initial and secondary I, respectively. The relation between initial-secondary I and time was quantified by linear regression, and the equations of the best curve fitting (solid black lines) were illustrated in Figures S5-S7 in the SI. In addition, the slope (s) and intercept (b) of each line were reported in Table 10. The slope (S_i and S_s) and the intercept (b_i and b_s) of the initial and secondary I, as critical parameters for comparing the WA of samples, were also calculated and reported in Table 10.

According to the results, MC2 had a lower S_i than MC3 and acted much better in terms of WA at a short exposure time. However, the S_s and b_s of these two LMCs (MC2 and MC3) were higher than those of MC1. Consequently, latexes in LMCs caused to increase in WA due to the hydrophilic groups on their copolymer structure and the formed voids. The results of the early and final WA as a function of the square root of time were reported in Figure 5 and Table 11.

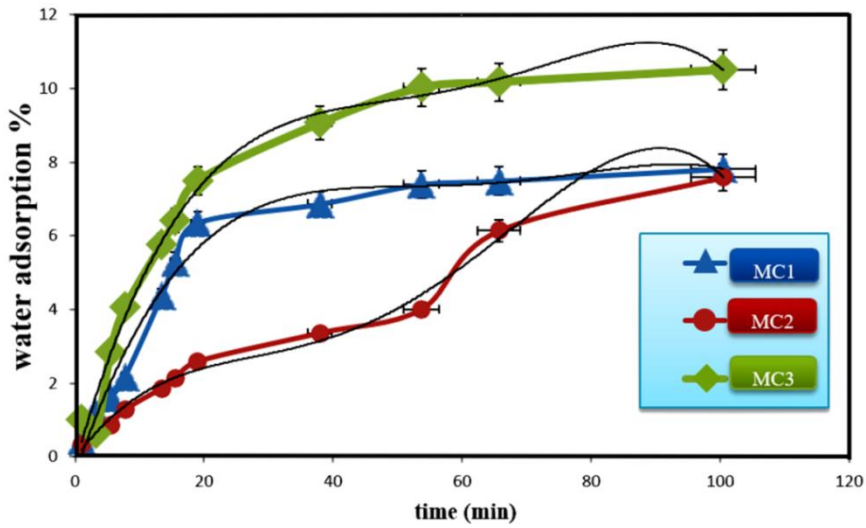

Figure 5: Early and final WA of samples vs. the square root time.

Table 10: The slope and intercept of initial, secondary, and total I.

Samples	Slope of initial I (s_i)	Intercept of initial I (b_i)	Slope of secondary I (s_s)	Intercept of secondary I (b_s)	Slope of total I (s)	Intercept of total I (b)
MC1	0.004	0.032	0.001	0.257	0.002	0.107
MC2	0.008	0.158	0.003	0. 594	0.004	0.315
MC3	0.012	0.292	0.006	0.292	0.006	0.506

Table 11: Early and final WA of samples.

Time (min)	Average WA of MC1	Average WA of MC2	Average WA of MC3
1	0.442	0.359	1.014
10	1.222	0.7	0.641
30 (early water absorption)	1.593	0.865	2.862
60	2.164	1.277	4.0624
180	4.355	1.862	5.781
240	5.283	2.126	6.431
360	6.35	2.590	7.497
1440	6.862	3.364	9.067
2880	7.398	4.006	10.032
4320	7.492	6.139	10.182
10080 (early water absorption)	7.817	7.593	10.511

The relation of WA vs. time for each sample was found, and the equations of the best curve fitting (solid black lines) were derived and were reported as equations 4, 5, and 6.

$$MC1: WA = -5E\text{-}07\ t^4 + 0.0001\ t^3 - 0.0129\ t^2 + 0.5216\ t - 0.475, \quad R^2 = 0.9801 \quad (4)$$

$$MC2: WA = -8E\text{-}07\ t^4 + 0.0001\ t^3 - 0.0088\ t^2 + 0.2454\ t - 0.0477, \quad R^2 = 0.9924 \quad (5)$$

$$MC3: WA = -2E\text{-}09\ t^5 - 2E\text{-}07\ t^4 + 0.0001\ t^3 - 0.0147\ t^2 + 0.6232\ t - 0.2058, \quad R^2 = 0.988 \quad (6)$$

The early WA of the samples was measured after 30 minutes of immersion in the water. According to the results, the WA of samples increased over time and finally reached a constant value. MC2 and MC3 had the lowest and the highest amount of early and final WA, respectively. Moreover, the differences in WA of MC1 and MC2 were significant until the sixth day; however, their WA reached the same value after six days. Subsequently, the chemical reactions and the film formation of latexes as additives were considered to justify the results. Figure 6 presents the mechanism of latex film formation (LFF) on the substrates, such as hydrated and non-hydrated cement particles.

In general, the film formation of latexes on the surface has four main steps: Flocculation of latex particles (LPs), Formation of the close-packed structure of LPs, Water molecules drainage from LPs, and Coalescence of LPs. After these steps, latex films form on the substrate [36-38]. Furthermore, the Cement hydration reaction occurs during the mixing cement, water, and latex in addition to the LFF [36, 39-40]. Figure 7 displays what happens after mixing sand, cement, water, and latex to achieve a coherent concrete structure schematically.

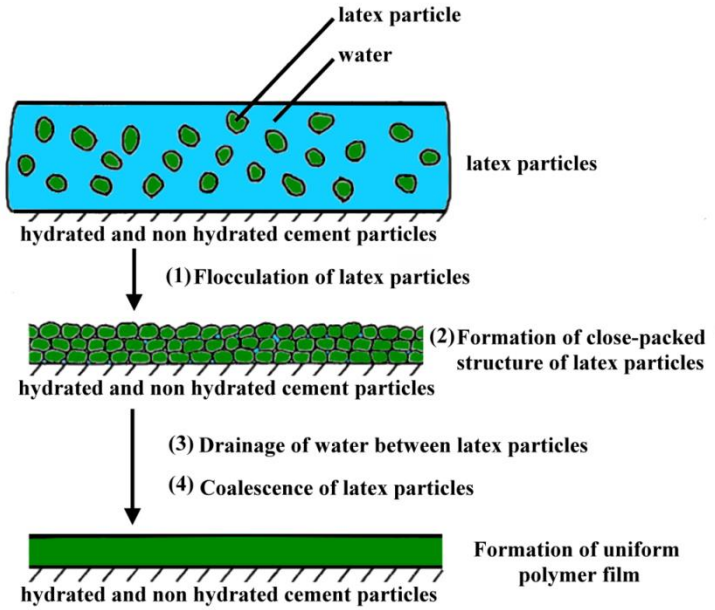

Figure 6: Schematic mechanism of latex film formation on the substrate [36].

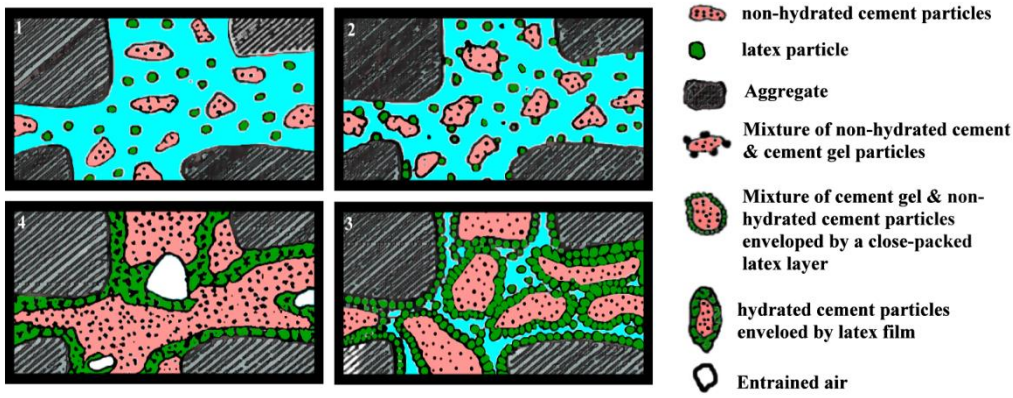

Figure 7: Schematic mechanism of LFF on hydrated and non-hydrated cement particles [38].

According to Figure 7, the hydration reaction occurs between cement and water after mixing latex, water, aggregates, and cement particles. A yogurt-like thin layer on the hydrated and non-hydrated cement particles is formed by latex. Therefore, a less porous structure with higher tortuosity can be prepared by incorporating latex in concrete. Furthermore, carboxylated latexes can react with hydrated particles and produce a three-dimensional network structure, as figured out in Figure 8 [35, 36, 38].

MFFT of latexes is one of the most important characteristics determining the LFF conditions. The higher MFFT leads to a slower film formation rate [36, 37]. It seems that the MFFT of latexes can justify the achieved results. It can be explained that if the MFFT of the latexes is less than the ambient temperature during the concrete mixing, the latex films quickly cover the surface of the non-hydrated cement particles. Consequently, the hydration reaction of the cement particles cannot occur completely, and the concrete faces the retardation effect. Hence, a concrete mixture without a coherent structure will be manufactured. Therefore, it can be explained that LFF happened fast on the non-hydrated cement particles of MC4

contained ASL-1 with low MFFT (~ 0 °C) compared to the ambient temperature, which prevented the hydration reaction. Due to the high MFFT of ASL-3, the LFF of MC2 was carried out slowly, and the cement particles were allowed to react completely with water molecules. Therefore, MC2 was found to have higher performance in WA, chloride migration, carbonation, and mechanical tests due to the complete hydration reaction and appropriate film formation of ASL-3on the hydrated cement particles. The LFF on cement particles was observed by SEM and Si X-ray mapping, displayed in Figure 9.

Since latexes had no Si element in their structures, Si X-ray mapping micrographs were considered to signify the location of latex films. It was detected in Figure 9 that latex films in MC2 are uniform and smooth, while non-hydrated cement particles in MC3 have incoherent latex coatings. In addition, it was concluded that the uniformity and thickness of latex films in the concrete composition depend on the MFFT of latexes. These results agreed with previous studies [39, 40]. It is noteworthy that the slow and uniform LFF on the hydrated cement particles can improve the penetration resistance to the chloride and carbonate ions in aggressive conditions due to the uniform ionic groups ($-COO^-$) exiting in the latex structure.

Furthermore, it can be concluded that the MFFT of latexes has a direct relationship with the fluency of fresh mortars and concrete, so MC4 containing ASL-1 with the lowest MFFT (~ 0 °C) and MC2 containing ASL-3 with the highest MFFT (~ 25 °C), had the lowest (70 mm) and the highest (185 mm) slump value, respectively. Hence, latexes with high MFFT can increase the service time or pot life of fresh LMCs. Moreover, the compressive strength of the LMC samples containing ASL with low MFFT was reduced because of the LFF on the non-hydrated particles and the prevention from the hydration reaction evolution, which needs water penetration into the cement particles. On the other hand, LMCs containing ASL with high MFFT had better compressive strength compared to MC1.

MC2 manufactured by carboxylated ASL provided improved splitting TS compared to the ordinary concretes. It can be explained by forming the three-dimension chemical bonding structure between the carboxylate group ($-COO^-$) and Ca^{+2} or Si-O-Si, according to Figure 8. Therefore, the latex films cover the surfaces of the hydrated crystals and fill the cracks and pores. Accordingly, MC2 had the highest ion penetration resistance, slump, compressive, splitting TS, and the lowest WA among all LMCs. Its performance was significantly enhanced compared to the ordinary concrete sample due to its higher MFFT.

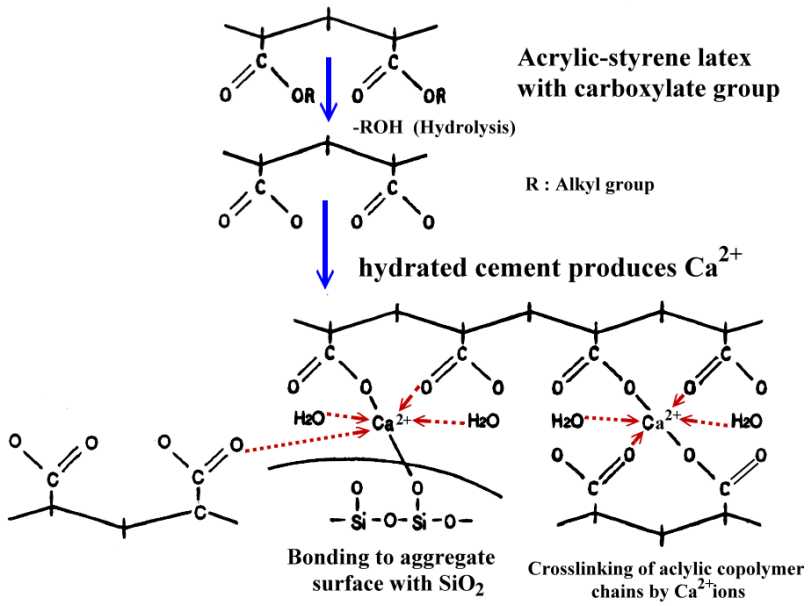

Figure 8: Schematic possible chemical reactions between carboxylic groups of latex and Ca^{+2} of hydrated cement or Si-O-Si of aggregates.

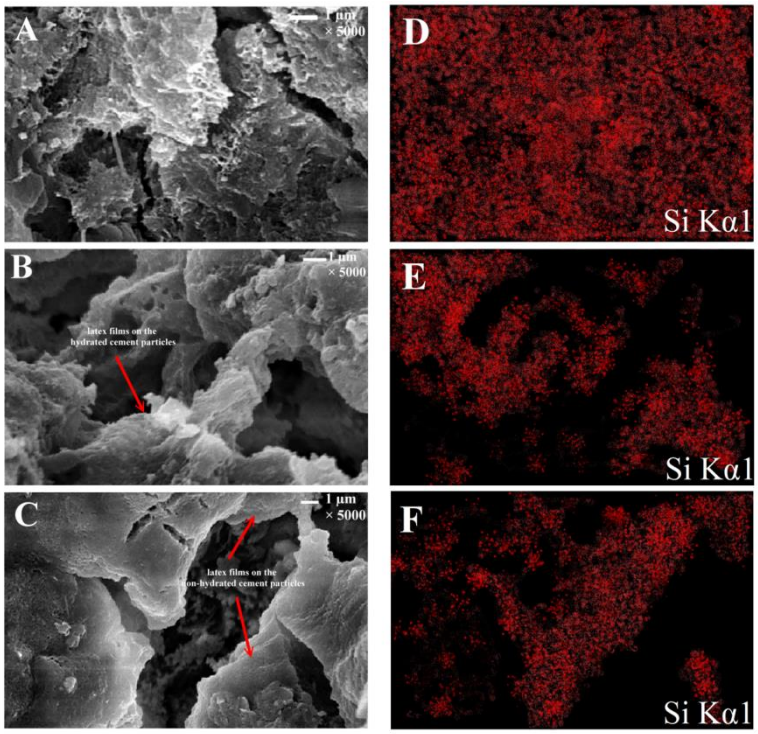

Figure 9: Morphology and Si X-ray mapping micrographs of the acrylic-styrene latex films on the hydrated and non-hydrated cement particles in MC1 (without latex films) (A & D), MC2 (B & E), and MC3 (C & F).

4. Conclusions

In this work, the effect of MFFT of ASL resins on the physical, mechanical, and durability properties, namely tensile and compressive strength, capillary and early-final WA, chloride and CO_2 diffusion, pH, density, and slump of the LMCs were investigated. The following conclusion can be drawn from the present study:

1. A four-step model proposed in this study can explain all possible physical and chemical events during the production process of LMC.
2. Latex resins with MFFT higher than operating temperature can act as a superplasticizer. It decreases the slump value without reducing workability.
3. Initial and final setting reaction rates of LMCs are dependent on the MFFT of the latexes.
4. Latex application in concrete admixtures reduces the compressive strength of LMCs, while ASLs with high MFFT rather than ambient temperature improves the TS compared to ordinary concrete.
5. Applying the latexes with high MFFT reduces chloride diffusion, carbonation, and WA at the aggressive condition due to the slower latex film formation on the hydrated and non-hydrated cement particles.
6. The temperature difference between ambient and MFFT of latex has determining effects on the final properties of LMCs. The latexes with high MFFT and alkaline conditions can be a promising candidates for the preparation of LMCs and can be applied in the RCs.

5. References

1. C. Jones, P. Subanen, W. M. Hale, Investigating concrete deterioration due to calcium oxychloride formation, *Constr. Build. Mater.*, 320(2022), 125600.
2. K. A. Erk, W. Siriwatwechakul, M. Wyrzykowski, D. Snoeck, Recent progress in superabsorbent polymers for concrete, *Cem. Concr. Res.*, 151 (2022), 106648.
3. Á. Salesa, J.A. Pérez Benedicto, D. Colorado Aranguren, P.L. López-Julián, L.M. Esteban, L.J. Sanz Baldúz, J.L. Sáez Hostaled, J. Ramis, D. Olivares, Physical mechanical properties of multi–recycled concrete from precast concrete industry, *J. Clean. Prod.*, 141(2017), 248-255.
4. H. Binici, O. Aksogan, Durability of concrete made with natural granular granite, silica sand and powders of waste marble and basalt as fine aggregate, *J. Build. Eng.*, 19(2018), 109-121.

5. Y. Tian, Ch. Dong, X. Cheng, Y. Wan, G. Wang, K. Xiao, X. Li, The micro-solution electrochemical method to evaluate rebar corrosion in reinforced concrete structures, *Constr. Build. Mater.*, 151(2017), 607-614.
6. K. Siamphukdee, F. Collins, R. Zou, Sensitivity Analysis of Corrosion Rate Prediction Models Utilized for Reinforced Concrete Affected by Chloride, *J. Mater. Eng. Perform.*, 22(2013), 1530-1540.
7. Sh. Mundra, M. Criado, S.A. Bernal, J.L. Provis, Chloride-induced corrosion of steel rebars in simulated pore solutions of alkali-activated concretes, *Cem. Concr. Res.*, 100(2017), 385-397.
8. J. Xiao, X. Long, W. Qu, L. Li, H. Jiang, Z. Zhong, Influence of sulfuric acid corrosion on concrete stress-strain relationship under uniaxial compression, *Measurement*, 187(2022), 110318.
9. S. Chinchón-Payá, C. Andrade, S. Chinchón, Indicator of carbonation front in concrete as a substitute to phenolphthalein, *Cem. Concr. Res.*, 82(2016), 87-91.
10. W. Xu, Yu. Li, H. Li, K. Wang, C. Zhang, Y. Jiang, S. Qiang, Corrosion mechanism and damage characteristic of steel fiber concrete under the effect of stray current and salt solution, *Constr. Build. Mater.*, 314(2022), 125618.
11. R. Wang, P. Wang, Function of styrene-acrylic ester copolymer latex in cement mortar, *Mater. Struct.*, 43(2010), 443-451.
12. M. Pei, W. Kim, W. Hyung, A.J. Ango, Y. Soh, Effects of emulsifiers on properties of poly (styrene-butyl acrylate) latex-modified mortars, *Cem. Concr. Res.*, 32(2002), 837-841.
13. M. L. Varghese, R. J. Babu, Effect of nano-silica on the physical, mechanical and thermal properties of the natural rubber latex modified concrete, *Indian J. Eng. Mater. Sci.*, 27 (2020), 1-14.
14. B.J. Lee, Y.Y. Kim, Durability of latex modified concrete mixed with a shrinkage reducing agent for bridge deck pavement, *Int. J. Concr. Struct. Mater.*, 12(2018), 1-9.
15. B. Liu, J. Shi, M. Sun, Z. He, H. Xu, J. Tan, Mechanical and permeability properties of polymer-modified concrete using hydrophobic agent, *J. Build. Eng.*, 31(2020), 101337.
16. S. Abdollahi Baghban, M. Khorasani, G. Mir Mohamad Sadeghi, Soundproofing performance of flexible polyurethane foams as a fractal object, *J. Polym. Res.*, 27(2020), 1-12.
17. L. K. Aggarwal, P. C. Thapliyal, S. R. Karade, Properties of polymer-modified mortars using epoxy and acrylic emulsions, *Constr. Build. Mater.*, 21(2007), 379-383.
18. M. Nodehi, S. E. Nodehi, Ultra high-performance concrete (UHPC): reactive powder concrete, slurry infiltrated fiber concrete and superabsorbent polymer concrete, *Innov. Infrastruct. Solut.*, 7(2022), 39.
19. S. Almeida AEF de, E.P. Sichieri, Experimental study on polymer-modified mortars with silica fume applied to fix porcelain tile, *J. Build. Environ.*, 42(2007), 2645-2650.
20. S. J. Kwon, M. Q. Feng, S. S. Park, Characterization of electromagnetic properties for durability performance and saturation in hardened cement mortar, *J. NDT E Int.*, 43(2010), 86-95.
21. S. Abdollahi Baghban, M. Ebrahimi, S. Bagheri-Khoulenjan, M. Khorasani, A highly efficient microwave-assisted synthesis of an LED-curable methacrylated gelatin for bio applications, *RSC Adv.*, 11(2021), 14996-15009.
22. S. Abdollahi Baghban, M. Ebrahimi, M. Khorasani, S. Bagheri-Khoulenjan, Self-stratifying behavior of a novel light-curable coating with gradient hydrophobic properties: Computational and experimental study, *Prog. Org. Coat.*, 159(2021), 106435.
23. S. Abdollahi Baghban, M. Ebrahimi, M. Khorasani, S. Bagheri-Khoulenjan, Design of different self-stratifying patterns in a VOC-free light-curable coating containing bio-renewable materials: Study on formulation and processing conditions, *Prog. Org. Coat.*, 161(2021), 106519.
24. J. M. Gao, C. X. Qian, B. Wang, K. Morino, Experimental study on properties of polymer-modified cement mortars with silica fume, *Cem. Concr. Res.*, 32(2002), 41-45.
25. M. Joo, Y. Ohama, K. S. Yeon, Strength properties of autoclaved and combined wet/dry-cured SBR-modified concretes using ground granulated blast-furnace slag, *Cem. Concr. Res.*, 56(2004), 513-521.
26. Z. Bahranifard, F.Farshchi Tabrizi, A.R. Vosoughi, An investigation on the effect of styrene-butyl acrylate copolymer latex to improve the properties of polymer modified concrete, *Constr. Build. Mater.*, 205(2019, 175-185.
27. V. Divry, A. Gromer, M. Nassar, C. Lambour, D. Collin, Y. Holl, Drying mechanisms in plasticized latex films: role of horizontal drying fronts, *J. Phys. Chem. B*, 120(2016), 6791-6802.
28. L. Tang, L. O. Nilsson, Rapid determination of the chloride diffusivity in concrete by applying an eElectric field, *ACI Mater. J.*, 89(1992), 49-53.
29. J. A. González, C. Andrade, C. Alonso, S. Feliu, Comparison of rates of general corrosion and maximum pitting penetration on concrete embedded steel reinforcement, *Cem. Concr. Res.*, 25(1995), 257-264.
30. M. Zailan Suleiman, R. Talib, M. Ramli, Durability and flexibility characteristics of latex modified ferrocement in structural development applications, *J. Eng. Des. Technol.*, 11(2013), 59-70.
31. N. Dave, V. Sahu, A.K. Misra, Development of geopolymer cement concrete for highway infrastructure applications, *J. Eng. Des. Technol.*, 18(2020), 1321-1333.
32. L. C. Page, N. R. Short, A. EI. Tarras, Diffusion of chloride in hardened cement pastes, *Cem. Concr. Res.*, 11(1981), 395-406.

33. J. Wei, X.X. Fu, J.H. Dong, W. Ke, Corrosion evolution of reinforcing steel in concrete under dry/wet cyclic conditions contaminated with chloride, *J. Mater. Sci. Technol.*, 28(2012), 905-912.
34. A. Beglarigale, H. Yazıcı, Electrochemical corrosion monitoring of steel fiber embedded in cement-based composites, *Cem. Concr. Compos.*, 83(2017), 427-446.
35. F. Moodi, A. Kashi, A.A. Ramezanian pour, M. Pourebrahimi, Investigation on mechanical and durability properties of polymer and latex-modified concretes, *Construct. Build. Mater.*, 191(2018), 145-154.
36. A. Shadmani, B. Tahmouresi, A. Saradar, E. Mohseni, Durability and microstructure properties of SBR-modified concrete containing recycled asphalt pavement, *Constr. Build. Mater.*, 185(2018), 380-390.
37. K.W. Kim, C. Yu, J.W. Han, C. G. Park, Strength and durability of rapid set PVA fiber-reinforced LMC for pavement repair, *Polym. Polym. Compos.*, 27(2019), 179-188.
38. M. Wang, R. Wang, H. Yao, S. Farhan, S. Zheng, Z. Wang, C. Du, H. Jiang, Research on the mechanism of polymer latex modified cement, *Constr. Build. Mater.*, 111(2016), 710-718.
39. C. Miao, Q. Ran, J. Liu, Y. Mao, Y. Shang, J. Sha, New generation amphoteric comb-like copolymer superplasticizer and its properties, *Polym. Polym. Compos.*, 19(2011), 1-8.
40. R. Wang, P. M. Wang, Function of styrene-acrylic ester copolymer latex in cement mortar, *Mater. Struct.*, 43(2010), 443-451

How to cite this article:
S. Abdollahi Baghban, M. Khorasani, High Durable Latex-Modified-Concretes: The Effect of Minimum Film Formation Temperature of Acrylic-Styrene Latex. Prog. Color Colorants Coat., 16 (2023), 181-195.